Quasi-static motion of a new serial snake-like robot on a water surface: a geometrical approach

Xiao Xie, Johann Herault, Étienne Clement, Vincent Lebastard, Frédéric Boyer

Quasi-static motion of a new serial snake-like robot on a water surface: a geometrical approach.

Xiao Xie, Johann Herault[1], Étienne Clement, Vincent Lebastard, Frédéric Boyer

***Abstract*— This paper reports methods to compute the equilibrium stances of a new snake-like robot designed to stabilize its head on a free water surface. To adjust rapidly the stability of the robot, this bio-inspired robot can rotate independently each body-shell, and modify the level of immersion of each module. To predict the stable stance accessible by this additional degree of freedom, a model is developed to compute the equilibrium configurations of the robot from a given parametrization of the body shape. Then, an algorithm is introduced to compute a sequence of controlled body deformations, such that the head configuration relatively to the water surface remains unchanged. Finally, we explore in simulation stances and quasi-static gaits, and investigate to what extent the buoyancy and the body deformations can be used to stabilize the head of the snake-like robot.**

I. INTRODUCTION

Marine robots inspired by eels and aquatic snakes has emerged in academic contexts [1], [2], [3]. Still under development for industrial underwater applications [3], these hyper-redundant serial robots are particularly compact and manoeuvrable, and offer an alternative to standard unmanned water surface vehicles. Despite the high potential of these bio-inspired robots, these applications on water surface remains complex due to their precarious stability. Indeed, their slender morphology, which is the main asset of their announced performance, makes them particularly sensitive to rolling motions (solid rotation about the longitudinal axis). The net torque of the forces of buoyancy associated with certain stances can destabilize the robot, and produces high acceleration due to their small longitudinal moment of inertia. Hence, this rolling motion is considered to be the most dangerous degree of freedom. The problem of instability of planar swimming is particularly obvious when robots [5], as well as real snakes, swim at low velocity. This parasitic rolling motion is a serious impediment of the visual guidance of these bio-inspired robots, as well as the strong effects on the swimming performances [5]. However, stabilization of snake-like robot swimming on water surface is poorly documented, and most control-oriented models consider neutrally buoyant robot moving in a 2D plane, except in [15]. To prevent the rolling motion, the robot can be equipped with floaters or attached to cables, but these passive systems reduces the manoeuvrability of the robots.

To overcome these issues, the present article proposes an additional degree of freedom that stabilizes the rolling body motion while preserving the performance of the planar anguilliform gait. This new device allows to modify rapidly the immersed volume by a local controlled rolling motion on each module having triangular-like cross sections (see Fig. 1). This stabilization strategy is inspired from semi-aquatic snakes living on river surface, such as Cottonmouth [6]. These snakes deform actively their body shape, thanks to complex combinations of flexions and torsion, to monitor the surrounding environment. This active stabilisation relies on a control of the distribution of buoyancy forces along their slender body. Taking inspiration from these aquatic snakes [6], we aim to design a robot and its control to achieve stabilization on water surface via an active control of buoyancy forces. The long-term goal is to maintain a gaze control on water surface paving the way to visual servoing-based navigation of autonomous snake-like robots. However, this additional degrees of freedom makes the design and the control of the robot more complex. In practice, it raises the central issue: how can these internal degrees of freedom be combined to stabilize and control the head configuration while moving on a flat water surface? This paper is a first attempt to address this problem by investigating the effect of the body deformations on the stability.

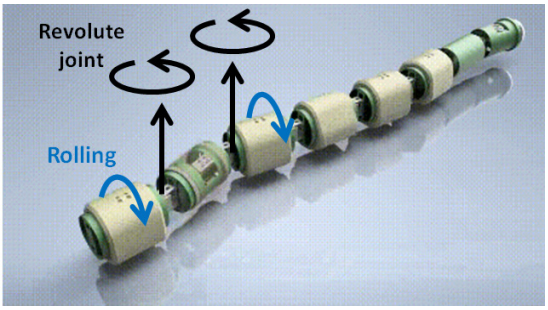

Fig. 1. The robot NATRIX with its distributed controlled rolling motions.

As a first step, we analyse the motion of the robot as a succession of static stable stances. This fictive quasi-static motion consists in neglecting all the inertial effects (fluid+body) as well as the viscous force produced by the fluid, so that no propulsion is allowed in our simplified model. The remaining forces are the gravity and the buoyancy. By artificially decoupling the locomotive gait and the buoyancy effects, we aim to identify the mechanism of stabilisation in the simplest framework. The quasi-static analysis will build the ground of more complex control laws accounting for the hydrodynamic and body inertia. Indeed, the stability of the robot can only be studied near a fixed point, which justifies the need for exploring all the possible stances at equilibrium. When inertia will be considered, this

[1] IMT Atlantique, LS2N, UMR CNRS 6004, F-44307 Nantes, France, johann.herault@imt-atlantique.fr

analysis will be helpful to plane real trajectories passing near this sequence of static stances, where the stability properties are already known.

To describe the configuration of the robot, we introduce the configuration space $\mathcal{C} = G \times \mathcal{S}$ ([7], [8]) given by the direct product of the workspace G, which is defined as the space of the head configuration g_0 taking values in the Lie group SE(3), and the shape space $\mathcal{S}$. Any pair $(g_0, \mathbf{q})$ is an element of the configuration space $\mathcal{C} = G \times \mathcal{S}$, a subspace of SE(3) $\times$ $\mathcal{S}$, which will be used to parametrize the configuration of the robot. In differential geometry, the space SE(3) $\times$ $\mathcal{S}$ is called a principal fiber bundle' [7] formed by the local direct product of a fiber SE(3) with the base manifold $\mathcal{S}$ (see Fig. 2). The forces of gravity and buoyancy being invariant by translation in the surface plane and rotations along the vertical direction, the system is unchanged if the head configurations are related by a rigid transformation on the water surface belonging to the group SE(2). Therefore, the configuration of the robot's head is given by the quotient space SE(3)/SE(2), such that the work space reads $G \simeq \mathrm{E}(1) \times S^2$. The Euclidean space E(1) stands for net vertical displacements (heaving), while S^2 represents the configuration space of rotations along vector tangent to the water surface (rolling and pitching). For the body shape, each segments having two revolute joints (rolling+flexural), the shape space is defined by its joint coordinates $\mathbf{q} \in \mathcal{S}$, with $\mathcal{S} = (S^1)^{2n}$, n being the number of segments.

To maintain a gaze control, our objective is to find a shape control law preserving static equilibrium. Such equilibria are reached when the robot is in a local minimum of potential energy determined by its coordinates $(g_0, \mathbf{q}) \in \mathcal{C}$ [9]. A sequence of static equilibrium can be seen as a trajectory connecting two points in the configuration space $\mathcal{C} = G \times \mathcal{S}$ with the control $\mathbf{q} \in \mathcal{S}$ (the base manifold) [8]. If g_0 is fixed in G, the set of all the body shapes $\mathbf{q}$ with the same equilibrium g_0 corresponds to a differentiable manifold $\mathcal{M}_{g_0}$ embedded in the shape space $\mathcal{S}$ (see Fig. 2). Hence, the sequence of equilibria can be parametrized by a trajectory belonging to the manifold $\mathcal{M}_{g_0}$. Therefore, our goal is to construct this trajectory on $\mathcal{M}_{g_0}$ by finding at each step the local minimum of potential energy. Rather than standard methods of constrained optimization problem embedded in a Euclidean space, we address this problem of optimization directly on the differentiable manifold, and construct this trajectory along "admissible" directions tangent to $\mathcal{M}_{g_0}$ [10]. Geometrically, our strategy consists in moving on the manifold $\mathcal{M}_{g_0}$ thanks to the properties of its local tangent spaces and its normal complements (see Fig. 2). This strategy is very similar to the geometrical concept of "connexion", which associates unequivocally each infinitesimal displacement on the base $\mathcal{S}$ with a corresponding displacement from one fiber to another [7]. However, the force of buoyancy being not left invariant, no connexion can be defined properly [7], [8]. Here, we will rather seek the admissible displacements on $\mathcal{M}_{g_0}$ that produces no variation of $g_0 \in G$ to remain on the manifold.

To construct this path on the set $\mathcal{M}_{g_0}$, we report two methods of optimization: a first method providing the equilibrium configuration of the head for a given body shape, and a second method to move on $\mathcal{M}_{g_0}$ along admissible directions. The main contribution of our work is to replace the time-integration, which disappears for quasi-static motion, by a line search strategies based on geometrical methods. For the first method, we use an algorithm of optimization on the Lie group to find the minimum of potential energy. For the second method, we use a local mapping from the tangent space of the locally smooth manifold $\mathcal{M}_{g_0}$ to elements on the manifold itself thanks to the projection-like retraction associated with a control system [10]. This paper is the continuation of our previous works on stability of continuous snakes [6]-[9] based on the Cosserat beam model, an approach which is now extended to our new discrete robot.

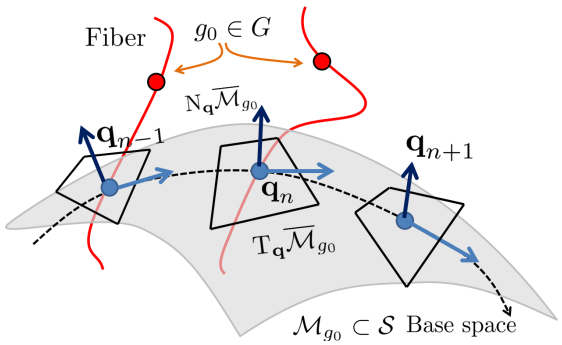

Fig. 2. Geometrical representation of the process of head stabilization in the principal fiber bundle SE(3) $\times$ $\mathcal{S}$. A sequence of equilibrium states with different body shapes $\mathbf{q}_n$ can be represented by any trajectory on the manifold $\mathcal{M}_{g_0}$, subset of the base state $\mathcal{S}$, while the head configuration g_0 remains unchanged in $G = \mathrm{SE}(3)/\mathrm{SE}(2)$.

The paper is organized as follows: Section II presents briefly the features of the robot and its geometrical model. In section III, the geometrical algorithm to compute the direct and inverse problem are reported. Section IV presents the results of these algorithms, and Section V discusses and concludes on the contributions of this work.

II. The Robot and its Geometrical Model

The bio-inspired robot NATRIX. The robot is similar to other planar snake-like robots [1], [2], [3] with serial revolute flexural joints. To control independently the swimming and the stability, an additional servomotor is fixed to each segment connecting two revolute joints, so that it can rotate the external shell of the module. This new local rolling motion is thus independent of the local bending, and preserves the planarity of the robot, as illustrated on Figs. 1 and 3. A similar concept has been recently used for terrestrial locomotion based on Archimedes' Screw [12], but it has never been proposed for aquatic snake-like robot. This robot is named NATRIX, and its design is detailed in an upcoming paper. The averaged robot's density is given by $\rho_{rob} = 312 \pm 2$ kg.m^{-3}. Each module has a triangular cross-section with rounded corners (see Figs. 1 and 5) to reproduce the snake morphology with a surface $S_{rob} = 11.3 \times 10^3$mm^2. The advantage of this triangular geometry is to decrease the height of center of

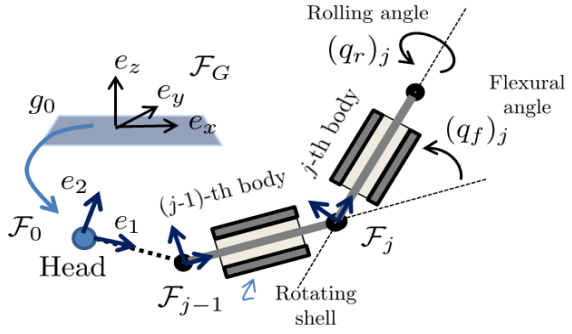

Fig. 3. Parametrization of the robot configuration

mass due to its large base section, and it provides large lateral surfaces to maximize thrust production. The length between two flexural joints is $L = 170$mm.

Geometrical model. To describe the orientation and position of our robot, a moving frame $\mathcal{F}_0$ is attached to the head. Its orientation and position are defined relatively to the water interface thanks to a Galilean frame $\mathcal{F}_G$ placed onto the surface (see Fig. 3). The configuration of $\mathcal{F}_0$ relative to $\mathcal{F}_G$ is given by the matrix $g_0 \in \mathbb{R}^{4\times4}$, the homogeneous representation of its transformation in SE(3), characterized by the rotation matrix $\mathrm{R}_0 \in$ SO(3) and the position vector $\mathbf{p}_0 \in$ E(3) [11]. The vector $\mathbf{q}$ defining the body shape is composed of the following joint coordinates (see Fig. 3): $\{(q_f)_k\}_{[1,n]}$ for the angles of the flexural joint, and $\{(q_r)_k\}_{[1,n]}$ for the angles of the rolling motion. To locate each module, a frame $\mathcal{F}_j$ is attached to the j-th flexural joint, the third axis being the axis of rotation. The configuration g_j relatively to the water frame $\mathcal{F}_G$ is given by

$$g_j = g_0 \left({}^0g_1\right) \dots \left({}^{j-1}g_j\right), \tag{1}$$

with ${}^{j-1}g_j$ the relative configuration of the j-th joint frame with respect to the $(j-1)$-th joint frame. The configuration ${}^{j-1}g_j$ is defined by the position vector $\left({}^{j-1}\mathbf{p}_j\right)^T = (L, 0, 0)$ and the rotation matrix

$${}^{j-1}R_j = \begin{pmatrix} \cos\left((q_f)_j\right) & -\sin\left((q_f)_j\right) & 0 \\ \sin\left((q_f)_j\right) & \cos\left((q_f)_j\right) & 0 \\ 0 & 0 & 1 \end{pmatrix}. \tag{2}$$

Then, the configuration $(g_{shell})_j$ of the shell of j-th module is deduced from the frame $\mathcal{F}_j$ by a longitudinal translation to the center of the module, followed by a longitudinal rotation given by the rolling angle with

$$(g_{shell})_j = g_j \begin{pmatrix} R_{shell}(j) & \mathbf{p}_{shell}(j) \\ 0 & 1 \end{pmatrix}, \tag{3}$$

with the position vector $\left(\mathbf{p}_{shell}\right)^T = (L/2, 0, 0)$, and the rotation matrix

$$R_{shell}(j) = \begin{pmatrix} 1 & 0 & 0 \\ 0 & \cos((q_r)_j) & -\sin((q_r)_j) \\ 0 & \sin((q_r)_j) & \cos((q_r)_j) \end{pmatrix}. \tag{4}$$

Hydrostatic forces. In a previous paper [9], we have introduced a model to compute the immersed volume of a solid body based on its configuration g relative to the surface. We review here briefly the method. For one given cross-section of a module, the air-water interface is given by the parametric equation $p_z + R_{32}Q_2 + R_{33}Q_3 = 0$, defining the waterline, with Q_1, Q_2, Q_3 the coordinates of a point in the local section frame (section 3.2 in [9]), and $R_{i,j}$ the component of the rotation matrix of the considered cross-section. According to the different cases of intersection between the water and the cross-section of the module, the immersed surface and its barycenter can be numerically computed for a triangular cross-section. Then, we compute the immersed volume of one module by integrating numerically the contribution of all the immersed surfaces. Finally, we can evaluate numerically the net potential energy $U(g_0, \mathbf{q}_0)$ of the robot by summing the potential energy of each module, and the net wrench $\mathbf{W}$, which has only three non-zero components in the frame $\mathcal{F}_G$: the vertical force F_z and the transversal torque Γ_x and Γ_y. We write $\tilde{\mathbf{W}}^T = (F_z, \Gamma_x, \Gamma_y)$ the reduced wrench with these three components.

III. The algorithms

Now, we introduce two methods to find and then move on the manifold $\mathcal{M}_{g_0}$ corresponding to all the elements $\mathbf{q} \in \mathcal{S}$ satisfying $\tilde{\mathbf{W}}(g_0, \mathbf{q}) = \mathbf{0}$ for a given g_0. First, we seek the root of $\tilde{\mathbf{W}}$ for a fixed body shape $\mathbf{q}$ thanks to a sequence of head configurations $\{(g_0)_n\}$ indexed by n so that $\tilde{\mathbf{W}}_n \to \mathbf{0}$ when n increases. To find the root, a gradient descent method adapted to the geometry of the Lie group SE(3) is used. We define an update formula to pass from a head configuration $(g_0)_n$ to $(g_0)_{n+1}$, such that the energy decrease satisfies the Armijo rule [13]. To preserve the structure of the Lie group SE(3), the update formula is a left matrix multiplications, and reads: $(g_0)_{n+1} = A_n\ (g_0)_n$ with the matrix $A_n \in$ SE(3) given by

$$A_n = \exp\left(t_n\ \hat{\xi}_n\right), \tag{5}$$

The relative transformation A_n is defined from an unitary direction $\boldsymbol{\xi}_n = \mathbf{W}/||\mathbf{W}||$, and a step size t_n determined by the Armijo rule [13]. Then, the transformation A_n is computed thank to the exponential map, mapping an element from the Lie algebra $\hat{\xi}_n \in se(3)$ to an element of the group. After some iterations of the descent methods approaching the minimum, we accelerate the code via a second-order method based on a Netwon-Raphson algorithm. The reported method provides the equilibrium state, and gives the starting point in the configuration space G to move on $\mathcal{M}_{g_0}$.

Then, we want to move on the manifold $\mathcal{M}_{g_0}$ by modifying the body shape while preserving the head configuration $g_0 \in G$. To address this problem, we introduce the concept of retraction, which is used in differential geometry to construct a path from the elements of the tangent space of a smooth Riemannian manifold [10]. The simplest way to move on a manifold is to follow a geodesic curve on a manifold endowed by a Riemannian structure. However, finding these

geodesic curves for an arbitrary manifold can be computationally expensive providing this update exists. An alternative method consists in constructing an approximation of the geodesic curve, at least at order $o(t)$. This method called a retraction is a geometrical construction connecting two infinitesimally closed points of the manifold, so that it shares the two leading order properties of the Taylor expansion of a geodesic curve. A mapping $\mathbf{u} \mapsto \mathbf{R}(\mathbf{q}, u)$ from a tangent space $\mathrm{T}_{\mathbf{q}}\mathcal{M}_{g_0}$ into $\mathcal{M}_{g_0}$, with $\mathbf{q}$ and $\mathbf{R}(\mathbf{q}, \mathbf{u}) \in \mathcal{M}_{g_0}$, is a retraction if and only if the curve $\gamma(\mathbf{q}, \mathbf{u}, t) = \mathbf{R}(\mathbf{q}, t\mathbf{u})$ with $t \in \mathbb{R}^+$, satisfies

$$\gamma(\mathbf{q}, \mathbf{u}, 0) = \mathbf{q} \quad \text{and} \quad \gamma(\mathbf{q}, \mathbf{u}, 0)' = \mathbf{u}. \tag{6}$$

The reader can find in [10] a more formal definition of the retraction. Here, we use a projection-like retraction (also called orthographic retraction [10]) illustrated in Fig. 4 that is defined by

$$\mathbf{R}(\mathbf{q}, t\mathbf{u}) = \mathbf{q} + t\mathbf{u} + \mathbf{h}\left[t\mathbf{u}\right], \tag{7}$$

with $\mathbf{u} \in \mathrm{T}_{\mathbf{q}}\mathcal{M}_{g_0}$ and $\mathbf{h}$ a orthographic retractor belonging to the orthogonal complement $\mathrm{N}_{\mathbf{q}}\mathcal{M}_{g_0}$ of $\mathrm{T}_{\mathbf{q}}\mathcal{M}_{g_0}$, which are subspaces of $\mathcal{S}$. It is worth noting that the update defined by Eq. 7 doesn't require a manifold endowed with a Riemannian structure so that no metric is necessary in our approach, only an inner product given by the dot product of $\mathbb{R}^{2n}$. To identify the local tangent space and its complement, we compute the exact differential $\mathrm{d}\tilde{\mathbf{W}}$ of $\tilde{\mathbf{W}}$. Then, we state that for any variation on the set of equilibrium configurations, the variations of body shape $\delta\mathbf{q}$ and head configuration $\delta\tilde{\psi}$ (defined below) have to satisfy $\mathrm{d}\tilde{\mathbf{W}} = 0$, which reads

$$\left(\mathrm{D}_{\tilde{\psi}}\tilde{\mathbf{W}}\right)\delta\tilde{\psi} + \left(\mathrm{D}_{q}\tilde{\mathbf{W}}\right)\delta\mathbf{q} = 0, \tag{8}$$

with the jacobian matrices $\left(\mathrm{D}_{\tilde{\psi}}\tilde{\mathbf{W}}\right) \in \mathbb{R}^{3\times 3}$ and $\left(\mathrm{D}_{q}\tilde{\mathbf{W}}\right) \in \mathbb{R}^{3\times 2n}$. Equation 7 plays the role of a connection on a principal fiber bundel. However, the jacobian matrices depend on the configuration g_0, i.e. Eq. 8 is not left invariant, and doesn't define a connexion.

The matrix $\left(\mathrm{D}_{\tilde{\psi}}\tilde{\mathbf{W}}\right)$ is called the hydrostatic stiffness matrix, and it is computed from the variation of the head configuration δg parametrized by $\delta\hat{\psi} \in se(3)$ so that $\delta g_0 = \delta\hat{\psi} g_0$. We introduce the mapping $\delta\tilde{\boldsymbol{\psi}}^T = (\delta z, \delta\theta_x, \delta\theta_y) \mapsto \delta\boldsymbol{\psi}^T = (0, 0, \delta z, \delta\theta_x, \delta\theta_y, 0)$, with $\delta\boldsymbol{\psi}$ the coordinates of the twist. This transformation allows to map elements from $\mathbb{R}^3$ to se(3). For a stable equilibrium configuration, the opposite of the eigenvalues λ_i of $\left(\mathrm{D}_{\tilde{\psi}}\tilde{\mathbf{W}}\right)$ give the positive hydrodynamic stiffness characterizing the local stability of the equilibrium [14]. For a straight body (no bending), the eigenvalue associated with the eigenvector in the longitudinal direction $\mathbf{e}_1$ characterizes the stability of the rolling mode, while the two others eigenvectors correspond to two modes of oscillations coupling the heaving and the pitching. If one of the eigenvalues becomes positive, which corresponds to a negative stiffness, the equilibrium is unstable. Note that this matrix $\left(\mathrm{D}_{\tilde{\psi}}\tilde{\mathbf{W}}\right)$ is also used in the Netwon-Raphson method reported in the optimization on the Lie group.

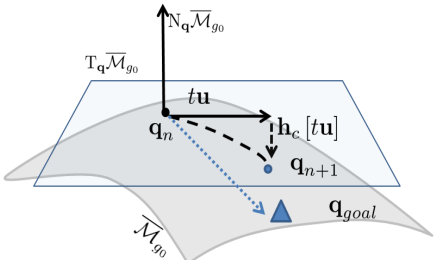

Fig. 4. Illustration of the retraction

The matrix $\left(\mathrm{D}_{q}\tilde{\mathbf{W}}\right)$ being rectangular, we perform a singular value decomposition (SVD) to compute its kernell, which is generated by the basis vectors $\{\mathbf{v}_{\|}\}$ spanning the local tangent space $\mathrm{T}_{\mathbf{q}}\mathcal{M}_{g_0}$. Then, the jacobian matrix $\left(\mathrm{D}_{q}\tilde{\mathbf{W}}\right)$ can be reduced to

$$\left(\mathrm{D}_{q}\tilde{\mathbf{W}}\right)_{\perp} = U_{\perp}\Sigma V_{\perp}^T \tag{9}$$

with Σ the non-zero diagonal matrix obtained by the SVD, and $V_{\perp}^T$ the matrix with the basis vectors $\{\mathbf{v}_{\perp}\}$, spanning the orthogonal complement $\mathrm{N}_{\mathbf{q}}\mathcal{M}_{g_0}$ of $\mathrm{T}_{\mathbf{q}}\mathcal{M}_{g_0}$ in the subspace of the joint coordinates. In our study, the rank of the matrix $\left(\mathrm{D}_{q}\tilde{\mathbf{W}}\right)_{\perp}$ is always 3.

A displacement $t\mathbf{u}$ on the tangent space produces a residual $\mathbf{W}\left(g_0, \mathbf{q} + t\mathbf{u}\right)$ of order $o(t)$. The orthographic retractor $\mathbf{h}$ is thus define to correct the small increase of wrench required to compensate any head variation, i.e. $\mathrm{d}\tilde{\psi} = \mathbf{0}$. To compensate this drift from the manifold $\mathcal{M}_{g_0}$, the orthographic retractor reads

$$\mathbf{h}\left[t\mathbf{u}\right] = -\alpha\left(\mathrm{D}_{q}\tilde{\mathbf{W}}\right)_{\perp}^{+}\mathbf{W}\left(g_0, \mathbf{q} + t\mathbf{u}\right) \tag{10}$$

with $\left(\mathrm{D}_{q}\tilde{\mathbf{W}}\right)_{\perp}^{+}$ the pseudo-inverse. The parameter $\alpha(\mathbf{u}, t)$ is a free real parameter, which is in practice close to one for $t \ll 1$, defining the step size along the admissible direction to come back to the manifold [10]. By construction, the retractor $\mathbf{h}\left[t\mathbf{u}\right]$ belongs to $\mathrm{N}_{\mathbf{q}}\mathcal{M}_{g_0}$ and is of order $O(t^2)$, so that the combination of Eqs. 7 and 10 is a retraction satisfying Eqs. 6. Now, the path is constructed by sequential updates, such that the n-th update is characterized by its parallel step direction $\mathbf{u}_n$ and step size t_n. To reach the goal body shape $\mathbf{q}_{goal}$, the unitary step direction $\mathbf{u}_n$ is constructed from the projection of the update goal direction $\mathbf{q}_{goal} - \mathbf{q}_n$ onto the tangent space, so that

$$\tilde{\mathbf{u}}_n = V_{\|}V_{\|}^T\left(\mathbf{q}_{goal} - \mathbf{q}_n\right), \quad \mathbf{u}_n = \frac{\tilde{\mathbf{u}}_n}{|\tilde{\mathbf{u}}_n|} \tag{11}$$

with $V_{\|}$ the rectangular matrix with the basis vectors $\{\mathbf{v}_{\|}\}$. The step size t_n is a slowly varying function of n, such that the system converges slowly to the goal.

IV. The Simulations

Thanks to the reported algorithms, we will investigate to what extent the buoyancy and the body deformations can be used to stabilize the head of the snake-like robot. Initially, the model of our robot is composed of 7 bodies:

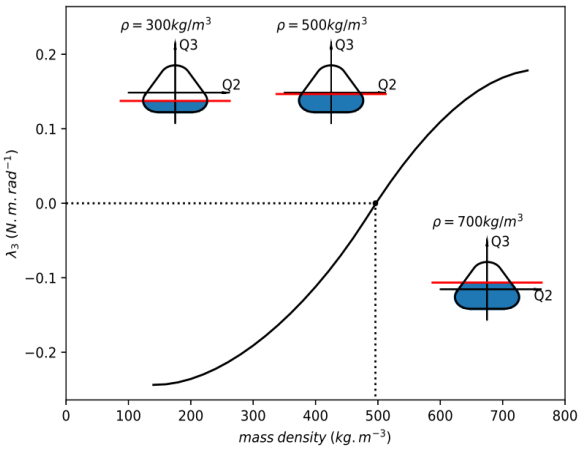

Fig. 5. Largest eigenvalue of the hydrodynamic stiffness matrix, corresponding to a rolling motion, as a function of the volumetric mass ρ for a straight body $\mathbf{q} = 0$.

one head plus 6 modules with 6 flexuraland rolling angles. First, we study the effect of the volumetric mass on the local stability of a straight robot ($\mathbf{q} = \mathbf{0}$) at equilibrium. In Fig. 5, we have reported the evolution of the largest eigenvalue λ_3 of the hydrostatic stiffness matrix, which is associated with a pure net rolling motion, as a function of the averaged volumetric mass of the robot. As expected, the level of immersion, illustrated by the embedded figures, goes up when the density increases. The eigenvalue, which is initially negative, also increases with the density, until the sign of the eigenvalue changes at $\rho_c = 497\text{kg.m}^{-3}$. At this critical point, the equilibrium becomes unstable: any infinitesimal rotation along the longitudinal axis will overturn the robot. This result confirms that the robot NATRIX has been designed to remain stable with a low density $\rho = 312\text{kg.m}^{-3}$ significantly smaller than ρ_c.

TABLE I

INTERMEDIATE FLEXURAL ANGLES FOR THE GOAL BODY SHAPE

t	$(q_1)_f$	$(q_2)_f$	$(q_3)_f$	$(q_4)_f$	$(q_5)_f$	$(q_6)_f$
0	30^o	-30^o	$-30\ ^o$	$0\ ^o$	$30\ ^o$	$30\ ^o$
T/4	$7\ ^o$	-40^o	$0\ ^o$	15^o	40^o	0^o
T/2	$-15\ ^o$	-27^o	$27\ ^o$	27^o	27^o	-27^o

This stability can also be improved by the anguilliform swimming gait. We compute a sequence of equilibrium states by moving on the manifold $\mathcal{M}_{g_0}$ via intermediate goal body shapes (see left Fig. 6) defined by a locomotive gait. The robot's density is fixed to 0.3. The values of the six flexural angles for the intermediate goal shapes are reported on table I for an half period, the setpoints for the other half are given by the opposite values. The rolling angles are set to zero. These goal shapes are used in Eq. 11 to define the admissible direction on $\mathcal{M}_{g_0}$. In Fig. 6 (right), we have reported the evolution of the flexural (thick curve) and rolling (dashed curve) angles of the second module as a function of the number of iterations, which can vary to reach the intermediate goal body shape. The flexural angle displays a sine-like function while the rolling angle remains null, as the other rolling angles. Indeed, the algorithm selects a path with solely flexions to preserve the stability. Then, the evolution of the eigenvalues of the hydrodynamic stiffness are reported on Fig. 6 (left) as a function of number of iterations of the process. The first iterations (up to 300) correspond to the transition from the straight configuration to the first goal body shape. All the eigenvalues remain negative, which implies that the quasi-static motion is always stable. However, their evolution differs significantly. The eigenvalues λ_1 and λ_2 (dashed curves) correspond to modes combining heaving and pitching motions. Their values are much smaller than the third eigenvalues, between one and two order of magnitude, and vary relatively slightly during the motion. The third eigenvalue λ_3, which corresponds mainly to a rolling motion, varies significantly during the gait. First, the stiffness is increased by a factor 8 when the body shape departs from the straight configuration, and reaches the first goal body shape. The smallest eigenvalue, which represents the most stable state, is reached at $t = T/4$ modulo $T/2$, and can be divided by two when the system is in the least stable state during the gait. This simulation demonstrates that the robot is particularly sensitive to the rolling motion, and its stability can significantly change during a gait.

We have tried to implement other goal body shapes with different setpoints for the rolling angles. The results were initially surprising: the rolling angles remain null regardless of the setpoints. The explanations is given by the physics of the system. When one module rolls, its immersed volume decreases, such that the equilibrium is no more satisfied. To balance this effect, the altitude of the head must decrease to dive and recover the immersed volume. However, this motion is forbidden in our algorithm: g_0 can't be changed. Therefore, the distributed rolling system can't be used when the pitching and the heaving of the head is not allowed.

To overcome this problem, we have added to our robot a neck between the head and the first body module. This neck has two pitch angles to compensate the pitching and the heaving of the body. This new robot model is composed of 8 bodies: one head, one neck and 6 modules with 5 flexural joints (one is replaced by the pitch joint) and 6 rolling joints. In Fig. 7, the eigenvalue λ_3 associated with the rolling motion are reported for three different shape control strategies. The first one (black curve) corresponds to a pure flexural motion without rolling angle ($q_r = 0$), which is the reference curve. Then, we have implemented a rolling motion inspired from aquatic snake, such that each shell rotates inward when the module departs from the straight configuration (see the small schema in the right corner of Fig. 7). This control law is surprisingly not effective since the eigenvalue (dot-dashed curves) remains above the reference curve (black curve). Finally, the last control law is an alternated rolling motion between each segment, such that the rolling angles changes its sign relatively to the previous rolling angle and also between each goal shape. Here, we

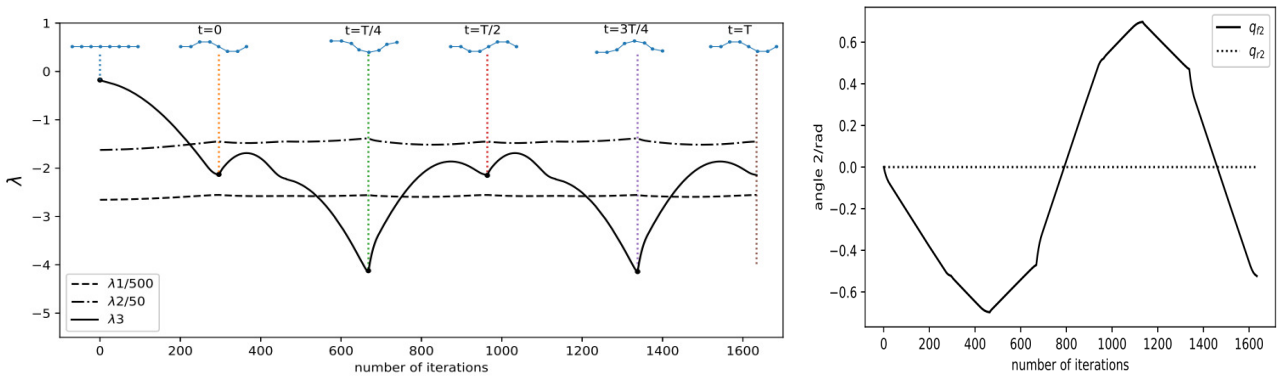

Fig. 6. (Left) Eigenvalues of the hydrodynamic stiffness matrix as a function of the iterations, which are required to undergo one period of a undulatory gait, illustrated by the intermediate body shapes. (Right) Evolution of the flexural and rolling joint angles of the second module as a function of the iterations.

observe a small improvement of the stability (the dotted curve having the smallest mean value) relatively to the pure flexural body motion.

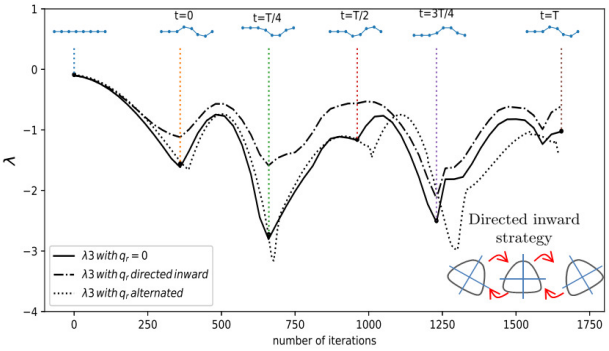

Fig. 7. Eigenvalue λ_3 of the hydrodynamic stiffness matrix as a function of the iterations for three different cases (see text).

V. CONCLUSIONS

The work presented in this paper represents the first steps in a program of research aiming to control the stability of snake-like robots swimming on water surface. First, we have introduced a new robot, called NATRIX, with an additional degree of freedom allowing to rotate the shell of each body module. To predict the stability of the robot, we have reported a method to deform the body shape while preserving the head configuration. Our study has demonstrated that the net rolling motion is the most dangerous degree of freedom for slender snake-like robot. Our simulations shows that the stability can be improved by the undulatory gait with a significant modulation of the hydrodynamic stiffness. A neck with two additional pitch angle is required to use the distributed rolling motion. Our simulations show that this simple additional degree of freedom can be easily controlled, and improve the stability of the robot. A step further would consist in seeking the optimal control of the body shape to provide a stable and controllable robot on water surface. Our future work will also consist in considering the dynamical aspects of the stability, and investigate to what extent the quasi-static stability can be used. Moreover, we are working on the instrumentation of the robot to compare these results with the reported results.

ACKNOWLEDGMENT

This work was supported by the French National Research Agency ANR (grant no. ANR-2019-CE33-0004- 01) and La Region Pays de la Loire (program "Étoile montante").

REFERENCES

[1] S. Hirose & H. Yamada,Snake-like robots [tutorial], IEEE Robotics, vol. 16 , n°11, pp. 88-98, 2009
[2] A. J. Ijspeert, A. Crespi, D. Ryczko, & J.-M. Cabelguen. From swimming to walking with a salamander robot driven by a spinal cord model. Science, 315(5817), 1416–1420. (2007)
[3] P. Liljebäck & R. Mill, Eelume: A flexible and subsea resident IMR vehicle. OCEANS 2017-Aberdeen, IEEE, 2017.
[4] A.J. Wiens & M. Nahon, Optimally efficient swimming in hyper-redundant mechanisms: control, design, and energy recovery, Bioinspiration & biomimetics, 7(4), 2012.
[5] M. Porez, F. Boyer, & A. J. Ijspeert, Improved Lighthill fish swimming model for bio-inspired robots: Modeling, computational aspects and experimental comparisons. The International Journal of Robotics Research, 33(10), 1322-1341, 2014.
[6] J. Herault, et al. Boyer, Standing on the Water: Stability Mechanisms of Snakes on Free Surface. In Conference on Biomimetic and Biohybrid Systems (pp. 165-175), 2020.
[7] F. Boyer, M. & Porez. Multibody system dynamics for bio-inspired locomotion: from geometric structures to computational aspects. Bioinspiration & biomimetics, 10(2), 025007, 2015.
[8] S. D. Kelly & R.M. Murray, Geometric phases and robotic locomotion. Journal of Robotic Systems, 1995, vol. 12, no 6, p. 417-431.
[9] J. Herault, A geometrically exact approach for floating slender bodies with finite deformations, Applied Research Ocean 101, 2020.
[10] P. A. Absil, & J. Malick, Projection-like retractions on matrix manifolds. SIAM Journal on Optimization, 22(1), 135-158, 20 , 2012.
[11] R. M. Murray, et al. A mathematical introduction to robotic manipulation. CRC press, 1994.
[12] D. Schreiber *et al*, ARCSnake: An Archimedes' Screw-Propelled, Reconfigurable Serpentine Robot for Complex Environments, 2020 IEEE (ICRA), 7029–7034, 2020.
[13] J. Nocedal, & Wright, S. Numerical optimization, 2006.
[14] T. I. Fossen. Handbook of marine craft hydrodynamics and motion control. John Wiley & Sons, 2011.
[15] E. Kelasidi, K. Y. Pettersen, & J. T. Gravdahl, Modeling of underwater snake robots moving in a vertical plane in 3D, 2014 IEEE IROS. (pp. 266-273). 2014.